JACS
JOURNAL OF THE AMERICAN CHEMICAL SOCIETY
pubs.acs.org/JACS
Article

Broadly Tunable Atmospheric Water Harvesting in Multivariate Metal−Organic Frameworks

Zhiling Zheng,[#] Nikita Hanikel,[#] Hao Lyu, and Omar M. Yaghi*

Cite This: https://doi.org/10.1021/jacs.2c09756
Read Online

ABSTRACT: Development of multivariate metal−organic frameworks (MOFs) as derivatives of the state-of-art water-harvesting material MOF-303 {[Al(OH)(PZDC)], where $PZDC^{2-}$ is 1*H*-pyrazole-3,5-dicarboxylate} was shown to be a powerful tool to generate efficient water sorbents tailored to a given environmental condition. Herein, a new multivariate MOF-303-based water-harvesting framework series from readily available reactants is developed. The resulting MOFs exhibit a larger degree of tunability in the operational relative humidity range (16%), regeneration temperature (14 °C), and desorption enthalpy (5 kJ mol^{-1}) than reported previously. Additionally, a high-yielding (≥90%) and scalable (∼3.5 kg) synthesis is demonstrated in water and with excellent space-time yields, without compromising framework crystallinity, porosity, and water-harvesting performance.

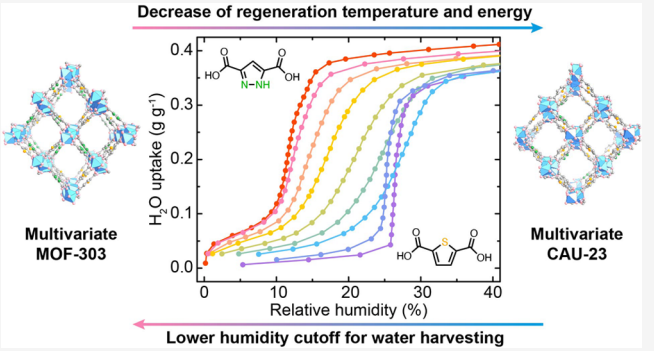

INTRODUCTION

Water is a valuable resource of unequal global distribution and increasing demand.[1] Its scarcity in many regions of the world has detrimentally affected the quality of life of many people.[2,3] The design of materials capable of harvesting water from air has been shown to be a potential solution for generating water, especially in arid climates.[4,5] Recently, metal−organic frameworks (MOFs) were successfully deployed for harvesting moisture from air.[5−11] To further advance this emerging field of research, it is imperative to establish strategies for generation of on-demand water-harvesting systems, which can be easily tailored to a variety of environmental conditions for efficient atmospheric water harvesting anytime of the year and anywhere in the world.[12]

In this report, we highlight how the multivariate strategy of making MOFs[13−15] provides a handle for controlling the hydrophilic nature of the pores and consequently the regeneration temperature and heat, as well as the humidity cutoff at which the MOF can operate. MOF-303 {[Al(OH)(PZDC)], where $PZDC^{2-}$ is 1*H*-pyrazole-3,5-dicarboxylate} is the basis of our study for its demonstrated success in water-harvesting desert trials.[10] Given the N(H) groups of the $PZDC^{2-}$ linker are the primary adsorptive sites for water molecules and the critical role the strength of this interaction plays in the building up of the water structure within the pores,[16] we sought to tune the hydrophilicity of these sites by introduction of thiophene-2,5-dicarboxylate (TDC^{2-}) along with $PZDC^{2-}$ in the MOF backbone. Based on these two linkers, nine multivariate PT-MOFs, formulated as $[Al(OH)(PZDC)_{1-x}(TDC)_x]$, covering the entire linker mixing range (x = 0, 0.125, 0.25, 0.375, 0.5, 0.625, 0.75, 0.875, and 1; Figure 1) were produced. These compounds have been made under both solvothermal and reflux-based conditions, and their structure, composition, and porosity were fully characterized. The power of the multivariate strategy is revealed by the water sorption behavior exhibited by this PT-MOF series, where it is possible to (i) tune and access a broader range of relative humidity at which the MOF operates and (ii) provide for a more energetically efficient water-harvesting process, as evidenced by lower regeneration temperatures and heats. These two findings far exceed what has already been reported and are suitable for water harvesting at arid conditions.[16,17] Additionally, we demonstrate the scalability of these multivariate compounds to the kilogram scale in water and with excellent space-time yields using readily available starting materials.

RESULTS AND DISCUSSION

Design Considerations and Synthesis. When considering the choice of the second linker for the MOF-303-based multivariate framework series, its availability and level of hydrophobicity are important factors. Additionally, the angle

Received: September 13, 2022

https://doi.org/10.1021/jacs.2c09756
J. Am. Chem. Soc. XXXX, XXX, XXX−XXX

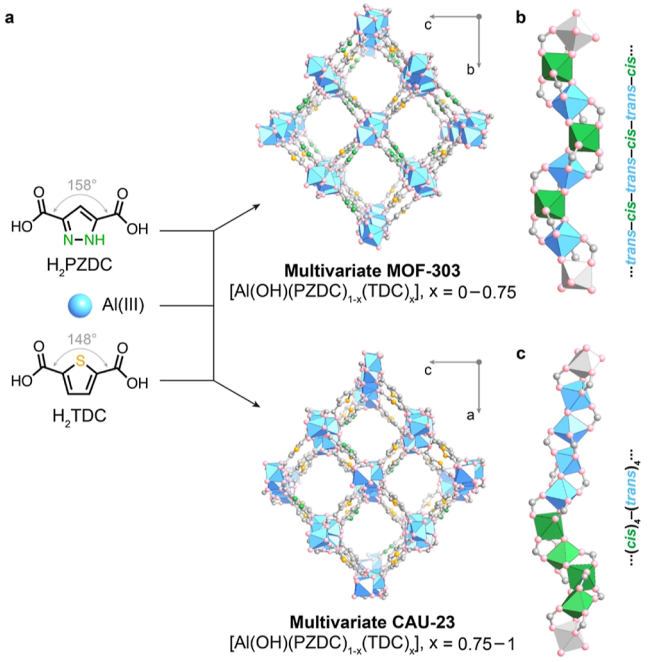

Figure 1. (a) Generation of multivariate MOFs from 1*H*-pyrazole-3,5-dicarboxylic acid (H_2PZDC) and thiophene-2,5-dicarboxylic acid (H_2TDC). Employing H_2PZDC or H_2TDC as linkers in single-linker MOFs results in MOF-303[9] or CAU-23,[21] which exhibit "infinite" SBUs consisting of (b) cis–trans-alternating or (c) $(cis)_4$–$(trans)_4$-alternating corned-shared AlO_6 octahedra, respectively. Dependent on the input linker ratio, base concentration, synthesis method, and reaction time, multivariate MOFs isostructural to MOF-303 or CAU-23 can be generated. The spatial linker distribution in the multivariate MOF series was not determined on the molecular level and is depicted arbitrarily. Al, blue octahedron in (a); trans-corner-shared AlO_6 octahedron, blue in (b,c); cis-corner-shared AlO_6 octahedron, green in (b,c); O, pink; C, gray; N, green; S, orange. H atoms are omitted for clarity.

between the carboxylic acid groups has to be similar to enable crystallization of both linkers in the same crystal lattice and avoid formation of a mixture of single-linker MOFs (Figure 1a).[18] Based on a search in the Cambridge Chemical Database using the Mogul software,[19,20] the angle between the carboxylic acid groups of protonated, uncoordinated H_2TDC is 147.7(17)°, thus exhibiting a deviation of 10° in comparison to H_2PZDC. This difference seems to be significant enough to result in single-linker MOFs of different topologies and space groups and with secondary building units (SBUs) of different stereochemistry.[9,21,22]

MOF-303 crystallizes in the monoclinic space group $P2_1/c$, and its rodlike SBU consists of cis–trans-alternating corned-shared AlO_6 octahedra.[9] On the other hand, CAU-23, [Al(OH)(TDC)], is reported in the orthorhombic space group $P2_12_12$ with its SBU comprising $(cis)_4$–$(trans)_4$-alternating corned-shared AlO_6 octahedra (Figure 1b,c).[21] Despite these structural differences, solvothermal synthesis of a multivariate MOF series covering the entire range of linker mixing ratios including the two single-linker frameworks MOF-303 and CAU-23 was carried out under aqueous conditions (Supporting Information, Sections 1 and 2). The nomenclature PTnm, which describes the molar input ratio of H_2PZDC to H_2TDC (n to m), will be used in the following to refer to the respective materials.

Structural and Compositional Characterization. Dependent on the linker ratio utilized in the synthesis, formation of two different phases was discovered using powder X-ray diffraction (PXRD) analysis of the synthesized multivariate PT-MOF series. Interestingly, at most of the input ratios of H_2PZDC (PT80 to PT26), phases isostructural to MOF-303 were observed, while only the compounds generated at low input ratios of H_2PZDC (PT17 and PT08) exhibited CAU-23-like structures (Figure 2a).

The composition of the multivariate PT-MOFs was probed using NMR spectroscopy, elemental analysis (EA), and scanning electron microscopy (SEM) coupled with energy-dispersive X-ray spectroscopy (EDS). Prior to subjecting the samples to NMR spectroscopy, the MOFs were thoroughly washed and then fully base-hydrolyzed using concentrated NaOD solution (Supporting Information, Section S4). Furthermore, the H_2PZDC content was extracted from the EA of activated MOF samples by using the N to S ratio. Both NMR and EA indicated formulaic behavior of the bulk PT-MOF samples, where the observed output ratio of H_2PZDC was proportional to the input ratio of the respective linker (Figure 2b). The presence of both linkers in the same crystallite was confirmed using SEM–EDS measurements on separated crystals of all members of the multivariate PT-MOF series (Figure 2c) as well as larger portions of the sample materials (Supporting Information, Section S6). EDS signals associated with Al, O, and C were observed in all crystallites, while the N signal diminished and the S signal increased with higher incorporation ratios of the TDC^{2-} linker. If present, both the N and S signals uniformly resembled the crystal outlines, thus indicating homogenous distribution of both linkers within the multivariate PT-MOFs. Interestingly, for some separated crystals, one could also observe different crystal morphologies when comparing the SEM micrographs of the MOF-303-like and the CAU-23-like phases (Figure 2c).

Thermal Stability and Porosity. Next, the thermal stability and porosity of the multivariate compounds were probed using thermogravimetric analysis (TGA) and nitrogen sorption analysis, respectively. Interestingly, all multivariate compounds isostructural to MOF-303 (PT80 to PT26) exhibited no weight loss up to ~400 °C under both argon and air atmospheres, while PT17 and PT08 displayed a slightly earlier onset of decomposition at both conditions (~375 °C; Supporting Information, Section S7). The Brunauer–Emmett–Teller (BET) surface areas and specific pore volumes decreased continuously from 1370 to 1220 $m^2\ g^{-1}$ and from 0.50 to 0.45 $cm^3\ g^{-1}$, respectively, with increasing incorporation of TDC^{2-} into the MOF structure, as one would expect considering the molecular weight difference between $PZDC^{2-}$ and TDC^{2-} (Supporting Information, Sections S8.1 and S8.2). The pore sizes were approximated to lie in the same range for all nine compounds (9.4–9.6 Å; Supporting Information, Section S8.2), as anticipated for frameworks constructed from linker molecules of similar length and without dangling side chains restricting the pore diameters.

Control of the Humidity Cutoff. The step of the water sorption isotherms of the multivariate PT-MOFs was shifted from 12% RH for PT80 (MOF-303) to 27% RH for PT08 (CAU-23; Figure 3a). Thus, with the combination of these two linkers, the tuning range was extended 50% compared to our previously reported multivariate MOF system.[17] The gravimetric water uptake capacity decreased from 0.45 to 0.42 $g\ g^{-1}$, which can, similar to the BET surface areas and specific pore

https://doi.org/10.1021/jacs.2c09756
J. Am. Chem. Soc. XXXX, XXX, XXX–XXX

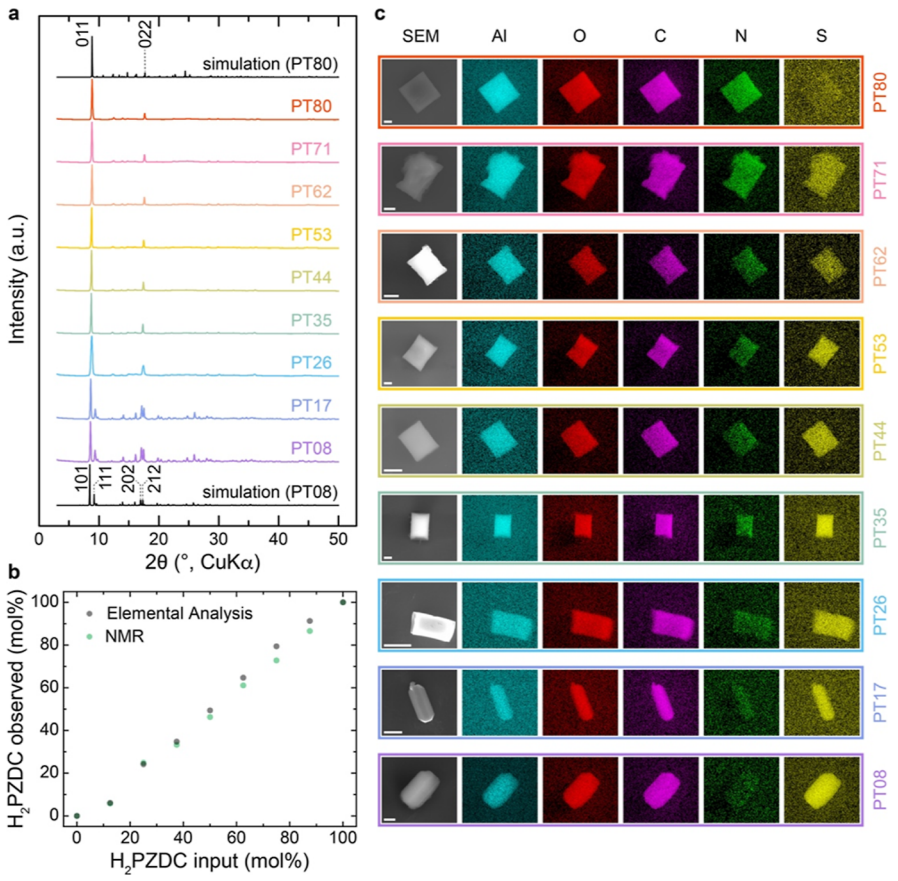

Figure 2. Structural and compositional characterization of the PT-MOF series synthesized under solvothermal conditions. (a) PXRD analysis using Cu Kα radiation. The simulated patterns at the top and bottom were generated using the fully water-loaded crystal structures of MOF-303 (PT80) and CAU-23 (PT08),[17,21] respectively. (b) Molar H_2PZDC linker ratios, as determined by NMR of thoroughly washed and fully hydrolyzed MOF samples, as well as N/S EA of activated frameworks, are plotted against the respective input linker ratio. (c) SEM with EDS of separated crystals of all members of the multivariate PT-MOF series. Prior to imaging, the crystals were washed with water and methanol and dried in vacuo. Scale bars: 1 μm.

volumes, be ascribed to the molecular weight difference between the two linkers. Only a minimal degree of hysteresis was observed for these MOFs (Figure 3b), which is an important prerequisite for energy-efficient atmospheric water harvesting. Interestingly, the structural type of the framework impacted the water sorption isotherm profile: While the CAU-23-type frameworks exhibited steep isotherm profiles, the compounds isostructural to MOF-303 displayed more gradual and shallow uptakes (Figure 3b), leading to the step position of PT26 at 28% being shifted to more hydrophobic values than PT08.

Tuning of the Heat of Adsorption. Additional water sorption data were collected on all compounds at 15 and 35 °C, which indicated consistent behavior across different temperatures (Supporting Information, Section S9.1). These data were used to estimate the differential enthalpies of adsorption Δh_{ads} using the Clausius−Clapeyron equation (Supporting Information, Section S9.2). The respective average values $\overline{\Delta h_{ads}}$ exhibited an impressive increase from −54 to −49 kJ mol^{-1} across the multivariate MOF series (Figure 3c). Considering that the heat of condensation of water at 25 °C is −44 kJ mol^{-1}, this corresponds to a decrease of the heat of adsorption penalty by a substantial 50%.

Modulation of the Regeneration Temperature. Furthermore, the multivariate approach allowed for a significant lowering of the desorption temperatures, as was estimated using water vapor desorption isobar measurements (Supporting Information, Section 9.3). At 1.70 kPa water vapor pressure, the desorption temperature could be shifted more than 14 °C using the multivariate approach (Figure 3d and Table S7). The trends in steepness and step positions between the water sorption isotherm profiles of the MOF-303-type and the CAU-23-type structures also translated to their isobaric curves, such that the isobaric curve of PT26 exhibited its desorption step at lower temperatures than PT08 but simultaneously required larger temperatures for complete desorption (Figure 3d and Supporting Information, Section 9.3).

Development of Scalable Synthetic Routes with High Space-Time Yields. Typically, the synthesis of MOF-303 was conducted at 1.5 base equivalents through unperturbed incubation of the reaction mixture in an isothermal oven overnight.[9] Employing these conditions to prepare multivariate MOFs resulted, at some linker mixing ratios, in compounds that exhibited water sorption isotherms with large hysteresis loops, which could only be removed through longer incubation times (2−4 days). At the same time, the yields never exceeded 50%, which was directly related to the base stoichiometry utilized during the synthesis (Table S1). Theoretically, to achieve quantitative yields of the compounds herein, one would require 3 base equivalents—2 for the full deprotonation of the dicarboxylic acid linker and 1 for the formation of the

https://doi.org/10.1021/jacs.2c09756
J. Am. Chem. Soc. XXXX, XXX, XXX−XXX

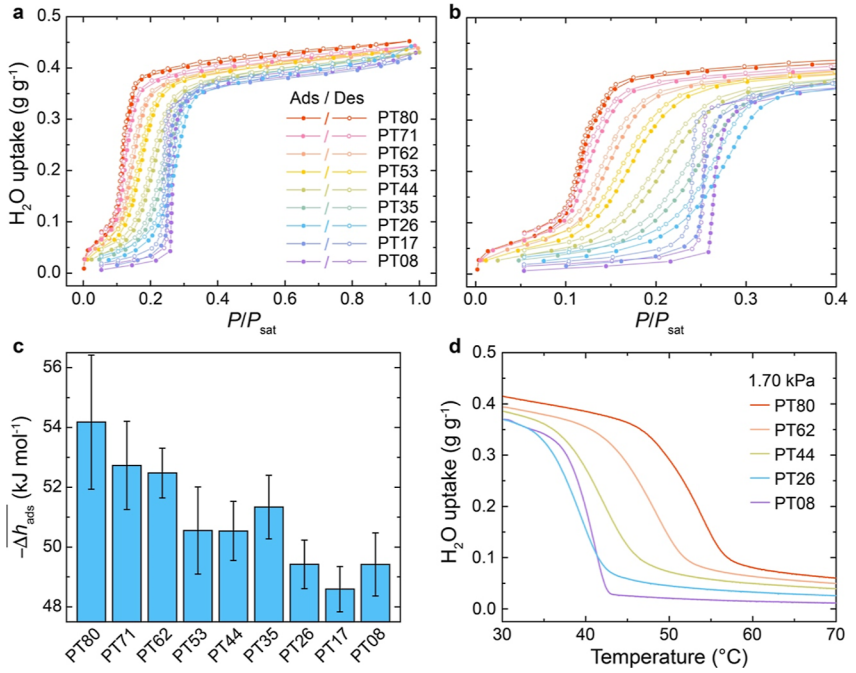

Figure 3. Water sorption properties of the multivariate PT-MOF series. (a) Full-range and (b) low-pressure region of the water sorption isotherms at 25 °C, where P is the water vapor pressure and P_{sat} is the saturation water vapor pressure. (c) Average negative differential adsorption enthalpy values $-\overline{\Delta h_{ads}}$ estimated from water sorption isotherms at 15−35 °C. The loading-dependent trends of Δh_{ads} and its respective standard errors can be extracted from Figures S68−S76. (d) Water vapor desorption isobar measurements of PT80, PT62, PT44, PT26, and PT08 at 1.70 kPa.

SBU. However, employing this base stoichiometry under solvothermal conditions resulted in MOFs with a substantial number of defects, as indicated by nonideal water sorption isotherms, which was likely related to insufficient equilibration under these unperturbed conditions (Figure S64). Finally, the solvothermal procedure was not scalable, thus preventing its practical use in an industrial setting.

To account for the aforementioned points, a reflux-based synthesis method under stirring and in the presence of 3 base equivalents was established (Figure 4a and Supporting Information, Section S1).[23] With this method, the reaction times could be reduced to a total of 5 h, and the yields were improved to ≥90% (Table S1), thus leading to space-time yield increases of 2 orders of magnitude for all multivariate PT-MOFs (Figure 4b and Table S2). The products, referred to as PTnm-HY (HY, high yield), exhibited high crystallinity, as was

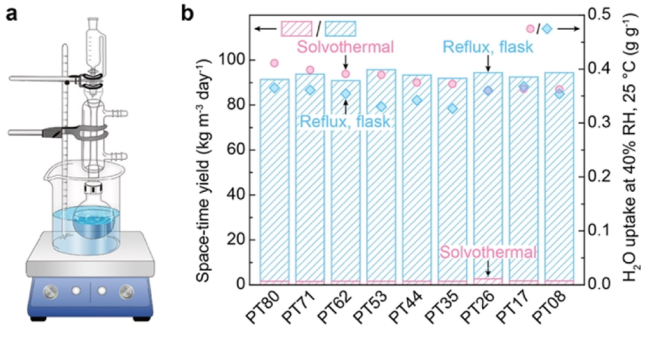

Figure 4. Synthesis of multivariate PT-HY-MOFs under reflux conditions in a flask. (a) Schematic representation of the experimental setup. (b) Comparison of the space-time yields and water uptakes at 40% RH and 25 °C for the multivariate PT-MOF series synthesized under solvothermal and reflux conditions in a flask.

verified by PXRD analysis (Figure S1), and proportionality between the linker input and output ratios according to NMR spectroscopy and EA (Figure 7b). The BET surface areas, estimated by using nitrogen sorption analysis, were comparable to the frameworks prepared under solvothermal conditions (1230−1370 m^2 g^{-1}; Supporting Information, Section 8.1). Importantly, the water sorption isotherm profiles indicated the same degree of tunability and similar water uptake capacities (Figures 4b and S65).

Time-Dependent Product Formation. Surprisingly, different products were obtained at a linker input ratio of 2 to 6 (H_2PZDC to H_2TDC) as a function of the reaction time. While PT26 prepared with the solvothermal procedure was isostructural to MOF-303 (Figure 2a), strikingly, the PXRD pattern of PT26-HY indicated a CAU-23-type structure (Figure S1). Formation of a product with a linker output ratio deviating from the input ratio, hinting at the formation of not fully equilibrated compounds, could be excluded by NMR spectroscopy and EA (Table S3). To further corroborate this observation, a series of compounds, termed PT26-HY-xh (x, refluxing time in hours), was prepared using different reaction times. Indeed, with increasing refluxing time, formation of a MOF-303-type product was prevalent (Figure 5a), while the output linker ratios for all multivariate PT26-HY-xh compounds were constant at all reaction times (Table S3). This behavior was further reflected in the step position and steepness of the respective water sorption isotherm profiles (Figures 5b and S66) and water desorption isobar profiles (Figure 5c), suggesting that PT26-HY-3h would be more suitable for water harvesting under arid conditions than PT26-HY-40h but would also require higher regeneration temperatures.

Mechanism of Formation. Motivated by the interesting time-dependent formation behavior of PT-26-HY, we decided

https://doi.org/10.1021/jacs.2c09756
J. Am. Chem. Soc. XXXX, XXX, XXX−XXX

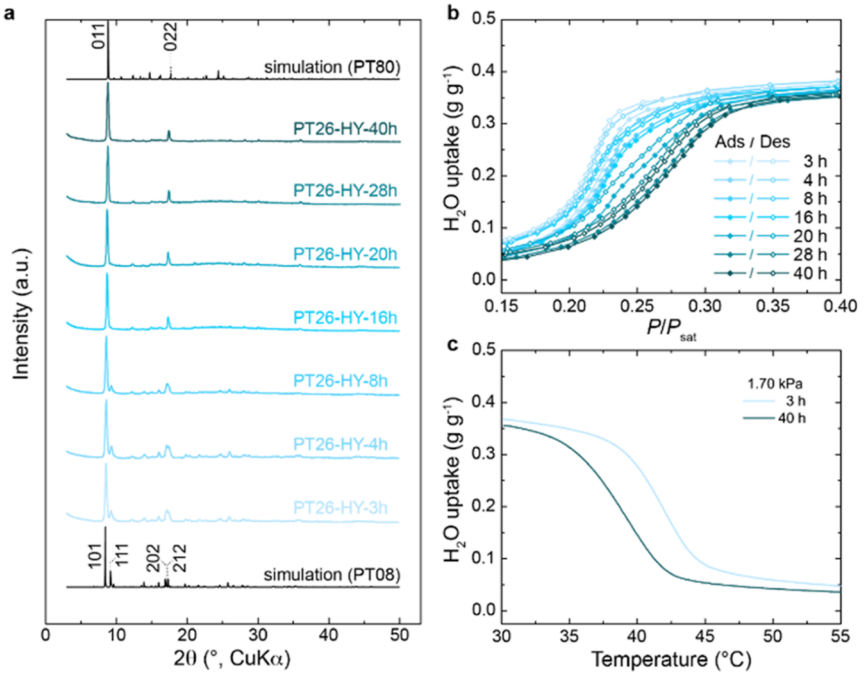

Figure 5. Structural characterization and water sorption properties of the multivariate PT26-HY-*x*h compounds synthesized under reflux for 3−40 h in a flask. (a) PXRD analysis using Cu Kα radiation. The simulated patterns at the top and bottom were generated using the fully water-loaded crystal structures of MOF-303 (PT80) and CAU-23 (PT08),[17,21] respectively. (b) Low-pressure region of the water sorption isotherms at 25 °C, where P is the water vapor pressure and P_{sat} is the saturation water vapor pressure. (c) Water vapor desorption isobar measurements of PT26-HY-3h and PT26-HY-40h at 1.70 kPa.

to probe its mechanism of inception. For that, we conducted PXRD analysis of samples formed at short reaction times (0−60 min refluxing time) and NMR spectroscopy of the respective thoroughly washed and fully base-hydrolyzed solid products as well as the associated reaction mixtures (Supporting Information, Section S5). It was apparent that after addition of the aluminum salt to the deprotonated linker solution, an amorphous, linker-containing product was formed, while the reaction mixture still contained relatively large amounts of both linkers. After only a few minutes of heating, a crystalline product was formed, and the linker concentrations in solution were rapidly depleted. The sample crystallinity increased upon further refluxing and slowly reached a steady degree within the first hour of the reaction, as has been observed in other studies probing the formation mechanism of aluminum MOFs built from rodlike SBUs at elevated temperatures.[24−26]

Scale-Up Synthesis of Multivariate MOFs. Encouraged by the promising results achieved through the reflux-based synthesis in a flask, the procedure was adapted to a 200 L-reaction vessel (Figure 6a and Supporting Information, Section S1). This approach provided ∼3.5 kg of activated MOF per reaction batch within 8 h (Figure 6b), thus resulting in more than doubling of the space-time yields compared to the flask-based synthesis (Table S2). The products were highly crystalline (Figure S2), exhibited formulaic behavior pertaining to the linker output ratios (Figure S7c), and displayed high BET surface areas in the range of 1120−1390 $m^2 g^{-1}$. Similar to the products obtained on a small scale, water sorption analysis revealed high tunability and water uptake capacities for these multivariate MOFs prepared at scale (Figures 6b and S67).

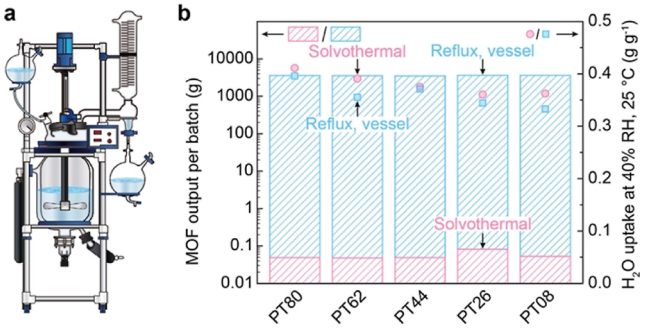

Figure 6. Synthesis of multivariate PT-MOFs under reflux conditions in a reaction vessel. (a) Schematic representation of the experimental setup. (b) Comparison of the MOF outputs per batch and water uptakes at 40% RH and 25 °C for the multivariate PT-MOF series synthesized under solvothermal conditions and reflux conditions in a reaction vessel.

CONCLUDING REMARKS

This study demonstrated a multivariate MOF system based on readily available starting materials. The resulting frameworks displayed an even broader range of tunability in the humidity range of atmospheric moisture uptake, regeneration temperature, and enthalpy of adsorption. Taken together, these advancements led to a more energy efficient and versatile water-harvesting system under arid conditions. Importantly, a synthesis procedure for these MOFs was developed to allow for their facile production at kilogram scale using water as a solvent, with high space-time yields and without major compromises to their water-harvesting performance. Overall, these findings are very encouraging considering the potential commercialization of the water-harvesting technology and the integration of these materials in large-scale atmospheric

https://doi.org/10.1021/jacs.2c09756
J. Am. Chem. Soc. XXXX, XXX, XXX−XXX

moisture extraction units to generate practical amounts of water anytime and anywhere.

■ ASSOCIATED CONTENT

Supporting Information

The Supporting Information is available free of charge at https://pubs.acs.org/doi/10.1021/jacs.2c09756.

Synthesis and characterization details of the multivariate PT-MOF compounds, including EA, PXRD patterns, NMR spectroscopy, SEM−EDS analysis, TGA curves, nitrogen sorption isotherms, as well as water sorption isotherms and isobars (PDF)

■ AUTHOR INFORMATION

Corresponding Author

Omar M. Yaghi − *Department of Chemistry, Kavli Energy Nanoscience Institute, and Bakar Institute of Digital Materials for the Planet, Division of Computing, Data Science, and Society, University of California, Berkeley, Berkeley, California 94720, United States; KACST−UC Berkeley Center of Excellence for Nanomaterials for Clean Energy Applications, King Abdulaziz City for Science and Technology, Riyadh 11442, Saudi Arabia;* orcid.org/0000-0002-5611-3325; Email: yaghi@berkeley.edu

Authors

Zhiling Zheng − *Department of Chemistry, Kavli Energy Nanoscience Institute, and Bakar Institute of Digital Materials for the Planet, Division of Computing, Data Science, and Society, University of California, Berkeley, Berkeley, California 94720, United States;* orcid.org/0000-0001-6090-2258

Nikita Hanikel − *Department of Chemistry and Kavli Energy Nanoscience Institute, University of California, Berkeley, Berkeley, California 94720, United States;* orcid.org/0000-0002-3292-5070

Hao Lyu − *Department of Chemistry and Kavli Energy Nanoscience Institute, University of California, Berkeley, Berkeley, California 94720, United States;* orcid.org/0000-0001-7393-2456

Complete contact information is available at: https://pubs.acs.org/10.1021/jacs.2c09756

Author Contributions

#Z.Z. and N.H. contributed equally to this work.

Notes

The authors declare the following competing financial interest(s): Omar M. Yaghi is co-founder of Water Harvesting Inc., aiming at commercializing related technologies. This work has been filed as US Provisional Patent Application No. 63/342,625.

■ ACKNOWLEDGMENTS

This material is based upon work supported by the Defense Advanced Research Projects Agency (DARPA) under contract HR0011-21-C-0020. Any opinions, findings, and conclusions or recommendations expressed in this material are those of the authors and do not necessarily reflect the views of DARPA. This study relied on the use of instruments located in the College of Chemistry Nuclear Magnetic Resonance (NMR) Facility, which are partially supported by NIH S10OD024998. We thank the NMR staff Dr. Hasan Celik and Dr. Alicia Lund for their assistance. Additionally, we thank Dr. Ha L. Nguyen, Dr. Wentao Xu, and Dr. Daria Kurandina for helpful discussions. We thank Dr. Xing Han and Zihui Zhou for assisting in assembling the reaction vessel and Dr. Ha L. Nguyen and Kelvin Kam-Yun Li from the Yaghi Research Group for help with the MOF synthesis at scale. Furthermore, we thank Dr. Xiaokun Pei and Saumil Chheda for crystallographic and computational efforts, respectively, aiming at further characterization of the compounds studied herein. N.H. thanks for the financial support through a Kavli ENSI Philomathia Graduate Student Fellowship and a Blavatnik Innovation Fellowship.

■ REFERENCES

(1) United Nations. *The United Nations World Water Development Report 2021: Valuing Water*; UNESCO: Paris, 2021.

(2) Mekonnen, M. M.; Hoekstra, A. Y. Four Billion People Facing Severe Water Scarcity. *Sci. Adv.* **2016**, *2*, No. e1500323.

(3) United Nations. *Sustainable Development Goal 6: Synthesis Report on Water and Sanitation*; New York, 2018.

(4) Elmer, T. H.; Hyde, J. F. Recovery of Water from Atmospheric Air in Arid Climates. *Sep. Sci. Technol.* **1986**, *21*, 251−266.

(5) Hanikel, N.; Prévot, M. S.; Yaghi, O. M. MOF Water Harvesters. *Nat. Nanotechnol.* **2020**, *15*, 348−355.

(6) Furukawa, H.; Gándara, F.; Zhang, Y.-B.; Jiang, J.; Queen, W. L.; Hudson, M. R.; Yaghi, O. M. Water Adsorption in Porous Metal−Organic Frameworks and Related Materials. *J. Am. Chem. Soc.* **2014**, *136*, 4369−4381.

(7) Kim, H.; Yang, S.; Rao, S. R.; Narayanan, S.; Kapustin, E. A.; Furukawa, H.; Umans, A. S.; Yaghi, O. M.; Wang, E. N. Water Harvesting from Air with Metal-Organic Frameworks Powered by Natural Sunlight. *Science* **2017**, *356*, 430−434.

(8) Kim, H.; Rao, S. R.; Kapustin, E. A.; Zhao, L.; Yang, S.; Yaghi, O. M.; Wang, E. N. Adsorption-Based Atmospheric Water Harvesting Device for Arid Climates. *Nat. Commun.* **2018**, *9*, 1191.

(9) Fathieh, F.; Kalmutzki, M. J.; Kapustin, E. A.; Waller, P. J.; Yang, J.; Yaghi, O. M. Practical Water Production from Desert Air. *Sci. Adv.* **2018**, *4*, No. eaat3198.

(10) Hanikel, N.; Prévot, M. S.; Fathieh, F.; Kapustin, E. A.; Lyu, H.; Wang, H.; Diercks, N. J.; Glover, T. G.; Yaghi, O. M. Rapid Cycling and Exceptional Yield in a Metal-Organic Framework Water Harvester. *ACS Cent. Sci.* **2019**, *5*, 1699−1706.

(11) Yilmaz, G.; Meng, F. L.; Lu, W.; Abed, J.; Peh, C. K. N.; Gao, M.; Sargent, E. H.; Ho, G. W. Autonomous Atmospheric Water Seeping MOF Matrix. *Sci. Adv.* **2020**, *6*, 1−9.

(12) Xu, W.; Yaghi, O. M. Metal−Organic Frameworks for Water Harvesting from Air, Anywhere, Anytime. *ACS Cent. Sci.* **2020**, *6*, 1348−1354.

(13) Deng, H.; Doonan, C. J.; Furukawa, H.; Ferreira, R. B.; Towne, J.; Knobler, C. B.; Wang, B.; Yaghi, O. M. Multiple Functional Groups of Varying Ratios in Metal-Organic Frameworks. *Science* **2010**, *327*, 846−850.

(14) Viciano-Chumillas, M.; Liu, X.; Leyva-Pérez, A.; Armentano, D.; Ferrando-Soria, J.; Pardo, E. Mixed Component Metal-Organic Frameworks: Heterogeneity and Complexity at the Service of Application Performances. *Coord. Chem. Rev.* **2022**, *451*, 214273.

(15) Furukawa, H.; Müller, U.; Yaghi, O. M. "Heterogeneity within Order" in Metal-Organic Frameworks. *Angew. Chem., Int. Ed.* **2015**, *54*, 3417−3430.

(16) Schlüsener, C.; Xhinovci, M.; Ernst, S.-J.; Schmitz, A.; Tannert, N.; Janiak, C. Solid-Solution Mixed-Linker Synthesis of Isoreticular Al-Based MOFs for an Easy Hydrophilicity Tuning in Water-Sorption Heat Transformations. *Chem. Mater.* **2019**, *31*, 4051−4062.

(17) Hanikel, N.; Pei, X.; Chheda, S.; Lyu, H.; Jeong, W.; Sauer, J.; Gagliardi, L.; Yaghi, O. M. Evolution of Water Structures in Metal-Organic Frameworks for Improved Atmospheric Water Harvesting. *Science* **2021**, *374*, 454−459.

(18) Schlüsener, C.; Jordan, D. N.; Xhinovci, M.; Matemb Ma Ntep, T. J.; Schmitz, A.; Giesen, B.; Janiak, C. Probing the Limits of Linker Substitution in Aluminum MOFs through Water Vapor Sorption Studies: Mixed-MOFs Instead of Mixed-Linker CAU-23 and MIL-160 Materials. *Dalton Trans.* **2020**, *49*, 7373−7383.
(19) Groom, C. R.; Bruno, I. J.; Lightfoot, M. P.; Ward, S. C. The Cambridge Structural Database. *Acta Crystallogr., Sect. B: Struct. Sci., Cryst. Eng. Mater.* **2016**, *72*, 171−179.
(20) Bruno, I. J.; Cole, J. C.; Kessler, M.; Luo, J.; Motherwell, W. D. S.; Purkis, L. H.; Smith, B. R.; Taylor, R.; Cooper, R. I.; Harris, S. E.; Orpen, A. G. Retrieval of Crystallographically-Derived Molecular Geometry Information. *J. Chem. Inf. Comput. Sci.* **2004**, *44*, 2133−2144.
(21) Lenzen, D.; Zhao, J.; Ernst, S.-J.; Wahiduzzaman, M.; Ken Inge, A.; Fröhlich, D.; Xu, H.; Bart, H.-J.; Janiak, C.; Henninger, S.; Maurin, G.; Zou, X.; Stock, N. A Metal−Organic Framework for Efficient Water-Based Ultra-Low-Temperature-Driven Cooling. *Nat. Commun.* **2019**, *10*, 3025.
(22) Tschense, C. B. L.; Reimer, N.; Hsu, C.; Reinsch, H.; Siegel, R.; Chen, W.; Lin, C.; Cadiau, A.; Serre, C.; Senker, J.; Stock, N. New Group 13 MIL-53 Derivates Based on 2,5-Thiophenedicarboxylic Acid. *Z. Anorg. Allg. Chem.* **2017**, *643*, 1600−1608.
(23) Zheng, Z.; Nguyen, H. L.; Hanikel, N.; Li, K. K.-Y.; Zhou, Z.; Ma, T.; Yaghi, O. M. High-Yield, Green and Scalable Methods for Producing MOF-303 for Water Harvesting from Desert Air. *Nat. Protoc.* **2022**, DOI: 10.1038/s41596-022-00756-w.
(24) Stavitski, E.; Goesten, M.; Juan-Alcañiz, J.; Martinez-Joaristi, A.; Serra-Crespo, P.; Petukhov, A. V.; Gascon, J.; Kapteijn, F. Kinetic Control of Metal-Organic Framework Crystallization Investigated by Time-Resolved In Situ X-Ray Scattering. *Angew. Chem., Int. Ed.* **2011**, *50*, 9624−9628.
(25) Embrechts, H.; Kriesten, M.; Hoffmann, K.; Peukert, W.; Hartmann, M.; Distaso, M. Elucidation of the Formation Mechanism of Metal−Organic Frameworks via in-Situ Raman and FTIR Spectroscopy under Solvothermal Conditions. *J. Phys. Chem. C* **2018**, *122*, 12267−12278.
(26) Salionov, D.; Semivrazhskaya, O. O.; Casati, N. P. M.; Ranocchiari, M.; Bjelić, S.; Verel, R.; van Bokhoven, J. A.; Sushkevich, V. L. Unraveling the Molecular Mechanism of MIL-53(Al) Crystallization. *Nat. Commun.* **2022**, *13*, 3762.

https://doi.org/10.1021/jacs.2c09756
J. Am. Chem. Soc. XXXX, XXX, XXX−XXX